Suzaku Observations of the Local and Distant Hot ISM

Randall K. Smith,[1,2] Mark W. Bautz,[3] Richard J. Edgar,[4] Ryuichi Fujimoto,[8]
Kenji Hamaguchi,[1] John P. Hughes,[5] Manabu Ishida,[7] Richard Kelley,[1]
Caroline A. Kilbourne,[1] K. D. Kuntz,[1,2] Dan McCammon,[6] Eric Miller,[3]
Kazuhisa Mitsuda,[8] Koji Mukai,[1] Paul P. Plucinsky,[4] F. Scott Porter,[1]
Steve L. Snowden,[1] Yoh Takei,[8] Yukikatsu Terada,[9] Yohko Tsuboi,[10] and Noriko Y. Yamasaki[8]

[1]*NASA/Goddard Space Flight Center, Code 662, Greenbelt, MD 20771, USA*
[2]*Department of Physics and Astronomy, The Johns Hopkins University, 3400 North Charles St., Baltimore, MD 21218, USA*
[3]*Kavli Institute for Astrophysics and Space Research, Massachusetts Institute of Technology,*
77 Massachusetts Avenue, Cambridge, MA 02139, USA
[4]*High Energy Astrophysics Division, Harvard-Smithsonian Center for Astrophysics, 60 Garden St., Cambridge, MA 02138, USA*
[5]*Rutgers, The State University of New Jersey, 136 Frelinghuysen Road, Piscataway, NJ 08854, USA*
[6]*Department of Physics, University of Wisconsin-Madison, 1150 University Avenue, Madison, WI 53706, USA*
[7]*Department of Physics, Tokyo Metropolitan University, Minami-Osawa 1-1, Hachioji, Tokyo 192-0397*
[8]*Department of High Energy Astrophysics, Institute of Space and Astronautical Science (ISAS),*
Japan Aerospace Exploration Agency (JAXA), 3-1-1 Yoshinodai, Sagamihara, 229-8510
[9]*Cosmic Radiation Lab., RIKEN, 2-1 Hirosawa, Wako, Saitama 351-0198*
[10]*Department of Physics, Faculty of Science and Engineering, Chuo University, 1-13-27 Kasuga, Bunkyo-ku, Tokyo 112-8551*
rsmith@milkyway.gsfc.nasa.gov

Abstract

Suzaku observed the molecular cloud MBM 12 and a blank field less than $3°$ away to separate the local and distant components of the diffuse soft X-ray background. Towards MBM 12, a local ($D \lesssim 275$ pc) O VII emission line was clearly detected with an intensity of 3.5 photons $\mathrm{cm}^{-2}\,\mathrm{s}^{-1}\,\mathrm{sr}^{-1}$ (or line units, LU), and the O VIII flux was < 0.34 LU. The origin of this O VII emission could be hot gas in the Local Hot Bubble (LHB), charge exchange within the heliosphere with oxygen ions from the solar wind (SWCX), or both. If entirely from the LHB, the emission could be explained by a region with emission measure of $0.0075\,\mathrm{cm}^{-6}\,\mathrm{pc}$ and a temperature of $1.2 \times 10^6\,\mathrm{K}$. However, this temperature and emission measure implies 1/4 keV emission in excess of observations. There is no evidence in the X-ray light curve or solar wind data for a significant contribution from geocoronal SWCX, although interplanetary SWCX is still possible. In any case, the observed O VII flux represents an upper limit to both the LHB emission and interplanetary SWCX in this direction. The blank field was observed immediately afterwards. The net off-cloud O VII and O VIII intensities were (respectively) 2.34 ± 0.33 and 0.77 ± 0.16 LU, after subtracting the on-cloud foreground emission. If this more distant O VII and O VIII emission is from a thermal plasma in collisional equilibrium beyond the Galactic disk, we infer it has a temperature of $(2.1 \pm 0.1) \times 10^6\,\mathrm{K}$ with an emission measure of $(4 \pm 0.6) \times 10^{-3}\,\mathrm{cm}^{-6}\,\mathrm{pc}$.

Key words: ISM: bubbles — plasmas — X-rays: ISM

1. Introduction

The soft (< 2 keV) diffuse X-ray background was a relatively early discovery of X-ray astronomy (see review by Tanaka, Bleeker 1977). Unlike the diffuse hard X-ray (> 2 keV) background, whose isotropy demonstrated it was dominated by extragalactic sources, the origin of soft component was and is more uncertain. While at high galactic latitudes extragalactic emission contributes to the observed flux, at lower latitudes the emission must be local to the Galaxy since at energies of 3/4 keV, absorption is significant (one optical depth is only $N_{\mathrm{H}} = 2 \times 10^{21}\,\mathrm{cm}^{-2}$). Despite this, both the Wisconsin M band (McCammon et al. 1983) and the ROSAT 3/4 keV (Snowden et al. 1995) surveys showed surprisingly little latitude dependence away from the Galactic bulge.

It is now known that at high latitudes, where N_{H} is generally less than $10^{21}\,\mathrm{cm}^{-2}$, $\sim 40\%$ of the 3/4 keV emission is due to AGN, and from the XQC sounding rocket flight we know that at least 42% of the high-latitude flux must be due to oxygen emission lines coming from $z < 0.01$ (McCammon et al. 2002) although it is not known if these are within the Galaxy or in the halo.

The situation in the Galactic plane is more confusing. Dwarf M stars must contribute some of the 3/4 keV emission (Kuntz, Snowden 2001), but at least 50% of the emission is of unknown origin (McCammon, Sanders 1990). O VII and O VIII contribute most of the line emission in the 3/4 keV band, although the fraction in lines versus continuum remains uncertain. Oxygen's dominance is due both to its large cosmic abundance (compared to other metals), and its strong emission lines at 0.57 keV (the O VII triplet from $n = 2 \rightarrow 1$) and 0.65 keV (the O VIII Ly α transition). Absorption limits the observed

in-plane 3/4 keV emission to regions within 1–2 kpc (assuming $\langle n \rangle \sim 1\,\mathrm{cm}^{-3}$ in the Galaxy).

Some of the 3/4 keV emission must be from the same source as the 1/4 keV X-ray background, which has been attributed to a combination of emission from a "Local Hot Bubble" (LHB) (Snowden et al. 1990) and charge exchange from solar wind ions (hereafter SWCX) (Cox 1998; Lallement 2004). In both cases, the X-rays must be truly "local", originating within $\sim 100\,\mathrm{pc}$ in the former case or within the Solar System in the latter.

To distinguish between the "local" 3/4 keV X-ray emission and the more distant Galactic and halo components, we used Suzaku to observe the nearby molecular cloud MBM 12 (= Lynds 1457), along with a nearby "blank-sky" position not occulted by the cloud. Earlier observations of MBM 12 obtained with ROSAT (Snowden et al. 1993, hereafter SMV 93) and Chandra observatory (Smith et al. 2005) had low spectral resolution (ROSAT) or were strongly affected by high background due to solar flares (Chandra). Our hope with this observation was to use Suzaku's low background, good spectral resolution, and sizable effective area × solid angle product to measure the components of both the local and more distant contributors to the 3/4 keV emission.

As described in Smith et al. (2005), the true distance to MBM 12 is uncertain, with estimates ranging from 60 ± 30 pc to 275 ± 65 pc. Our goal, however, is only to use MBM 12 as a curtain that separates local components such as the LHB and SWCX from more distant components such as a hot halo or extragalactic emission. It seems unlikely there is a significant component to the soft X-ray emission that is beyond the LHB but in front of MBM 12, so the distance uncertainty is not particularly important to this analysis. The total column density due to the MBM 12 cloud is also somewhat uncertain. We follow Smith et al. (2005), who argued for $N_{\mathrm{H}} = 4 \times 10^{21}\,\mathrm{cm}^{-2}$ as a reasonable value for the densest region of MBM 12. Although the Suzaku XIS 1 has more than four times the field of view of the Chandra ACIS-S3 ($17\farcm8 \times 17\farcm8$ versus $8\farcm5 \times 8\farcm5$), this is of similar size to the densest part of MBM 12 and so we expect a similar total column density. For the O VII and O VIII lines most relevant to our analysis the optical depths for this column density are 3.5 and 2.4, respectively. In addition, with a nearby off-cloud measurement, we will be able to directly determine the distant contribution and estimate its effect on the on-cloud emission.

ROSAT observations were only able to put a 2σ upper limit of $270\,\mathrm{counts}\,\mathrm{s}^{-1}\,\mathrm{sr}^{-1}$ on the 3/4 keV emission seen towards MBM 12 (SMV 93).[1] SMV 93 fit a "standard" 10^6 K collisional ionization equilibrium (CIE) LHB model (Raymond, Smith 1977) assuming a pathlength of ~ 65 pc, and found a good match to the observed 1/4 keV emission with an emission measure of $0.0024\,\mathrm{cm}^{-6}$ pc. This model generates only $\sim 47\,\mathrm{counts}\,\mathrm{s}^{-1}\,\mathrm{sr}^{-1}$ in the 3/4 keV band, primarily due to $\sim 0.28\,\mathrm{photons}\,\mathrm{cm}^{-2}\,\mathrm{s}^{-1}\,\mathrm{sr}^{-1}$ (hereafter LU, for "line units") generated by the O VII triplet (based on the ATOMDB ver. 1.3.1 atomic database). However, the ROSAT PSPC had little spectral resolution in this band and could not separate the O VII

and O VIII lines from the background continuum, and possible Fe L line emission.

Smith et al. (2005) used the Chandra ACIS instrument to redo the SMV 93 observations with higher spectral and spatial resolution. The results were affected by a large solar flare during part of the observation, which likely led to increased emission from SWCX [see Snowden et al. (2004) for more details on SWCX]. Smith et al. (2005) detected strong O VII and O VIII emission lines with surface brightnesses of $1.92^{+0.61}_{-0.60}$ and $2.35^{+0.59}_{-0.43}$ LU respectively, much larger than the prediction from SMV 93. The O VIII emission itself was also unexpected, as Smith et al. (2005) showed that it cannot come from any of the standard LHB models, either equilibrium or strongly recombining. They suggested that the observed O VIII emission was from the SWCX, although this could not be proven.

2. Observations

The molecular cloud MBM 12 was observed by Suzaku on 2006 February 3–6 for a total of 231 ks. The nominal pointing position was (RA, Dec) = $(02^{\mathrm{h}}56^{\mathrm{m}}00^{\mathrm{s}}, +19°29'24'',$ J2000) $[(l, b) = (159°2, -34°47)]$, corresponding to the most infrared-luminous and thus densest portion of the molecular cloud. Immediately thereafter (on 2006 February 6–8) an "off-cloud" pointing was obtained towards $(02^{\mathrm{h}}45^{\mathrm{m}}16^{\mathrm{s}},$ $+18°20'14''3,$ J2000) $[(l, b) = (157°3, -36°8)]$, a position $2°79$ distant from the cloud, for 168 ks. We present data primarily from the XIS instrument (Koyama et al. 2007), using the back-illuminated CCD XIS 1 which has the largest effective area at energies below 1 keV. The two fields of view are shown in figure 1, overplotted on the IRAS 100 μm image.

We used version 0.7 of the Suzaku data processing pipeline for our base dataset. The cleaned ver. 0.7 data are by default filtered to exclude times within 436 seconds of Suzaku passing through the South Atlantic Anomaly (SAA), and when Suzaku's line of sight is elevated above the Earth's limb by less than $5°$, or is less than $20°$ from the bright-Earth terminator. We decided to expand this to exclude events with Earth-limb elevation angle less than $10°$, as there were some excess events in the 0.5–0.6 keV band in the $5°$–$10°$ range. Finally, flaring pixels were removed using the cleansis tool with the default ver. 0.7 parameters. Although these are a small fraction of the total number of pixels on the CCD, they contribute a sizable background. In the case of the on-cloud data for XIS 1, just 1055 flickering pixels (out of $\sim 10^6$ total pixels) contributed $\sim 46\%$ of the total counts.

The bright intermediate polar XY Ari was serendipitously included in the on-cloud observations; this source will be discussed in a separate paper. XY Ari is sufficiently highly absorbed (Salinas, Schlegel 2004) that no photons below 1 keV are expected from the source. However, a smoothed image of the 0.4–1.0 keV band (see figure 2, left) shows low-energy emission from XY Ari, likely due to the tail of the CCD response curve. We therefore excluded a $2'$ radius region around XY Ari (marked with a red circle in figure 2, left) in order to reduce this background. This had the effect of substantially reducing the total background at all energies while excluding only a small fraction of the total $17\farcm8 \times 17\farcm8$ field. In addition, there were two other weaker sources found

---

[1]   We present all surface brightnesses in units of steradians, and note that $1\,\mathrm{sr} = 1.18 \times 10^7\,\mathrm{arcmin}^2$.
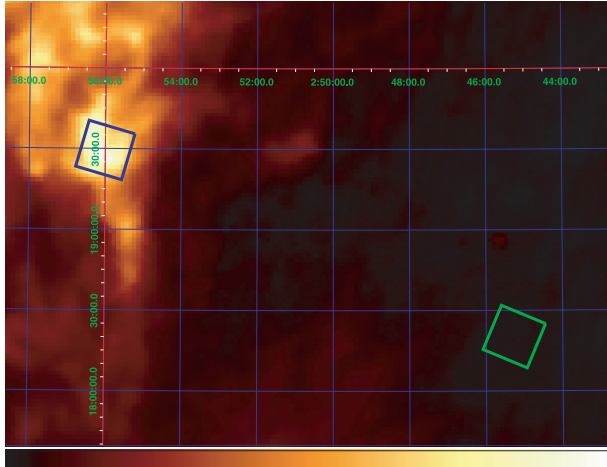
Fig. 1. Suzaku field of view for on-cloud (blue) and off-cloud (green) pointings, overlaid on the IRAS $100\,\mu$m survey image, which shows the bright emission from the MBM 12 molecular cloud.

which were also previously found in the Chandra observation of MBM 12. These are marked in figure 2 left with a $1'$ radius blue circle $(02\!:\!55\!:\!48,\,+19\!:\!29\!:\!12,\,\mathrm{J}2000)$ and a white circle $(02\!:\!55\!:\!51,\,+19\!:\!26\!:\!21,\,\mathrm{J}2000)$. Both had hard spectra with no significant flux below 1 keV in either the Suzaku or Chandra data. In the off-cloud data (figure 2 right) we discovered a bright source at $(02\!:\!45\!:\!09,\,+18\!:\!21\!:\!30,\,\mathrm{J}2000)$ (red circle) which does not appear in the ROSAT All-Sky Survey or any other catalog. We leave analysis of these sources for a future paper, and concentrate on the diffuse soft X-ray emission.

2.1. Background

As the goal of the observation was to extract the soft X-ray background, which fills the field of view, other background components cannot be estimated directly from the observation. Therefore our first focus was on understanding

the importance of the three major background components: particle contamination, scattered solar X-rays, and solar wind charge exchange. We did not exclude the corners of the detectors which contained the onboard calibration sources in our analysis, but instead fit these lines (which are all $> 1\,\mathrm{keV}$) as part of our source and background models.

2.1.1. Particle background

Suzaku is in a low-Earth orbit, so it is significantly shielded from the particle background that strongly affects XMM-Newton and Chandra. The effectiveness of this shielding is dependent upon the "cut-off rigidity" (COR) of the Earth's magnetic field, which varies as Suzaku traverses its orbit. During times with larger COR values, fewer particles are able to penetrate to the satellite and to the XIS detectors. We considered using the default value (COR > 4 GV) but finally chose to use a stronger constraint (COR > 8 GV) for both observations, as the lowest background was desired. This tighter constraint eliminates 27% (28.5 ks) of the total on-cloud observation time but 35% of all the XIS 1 counts. After this cut, we were left with 71.7 ks of "good" time for the on-cloud observation and 51.85 ks for the off-cloud pointing.

Although it is reduced by the Earth's magnetic field, Suzaku still has a noticeable particle background. Fortunately, we can estimate the background level quite accurately as a part of most observations is spent observing the Earth at night, and these data are a good proxy for the pure particle background. Phenomena such as aurorae have been observed to contribute X-rays to the Earth's night sky (Bhardwaj 2006), but these processes tend to be transient and thus are easily removed from the data. We used ∼ 400 ks of night Earth observations from the Science Working Group phase of the mission. The data were filtered to remove flares, and to ensure that Suzaku's line-of-sight elevation from the Earth limb was less than $-5°$ while observing the dark Earth. We also required the same cut-off rigidity constraint (COR > 8 GV) as used for the on- and off-cloud observations when extracting the particle background spectrum.
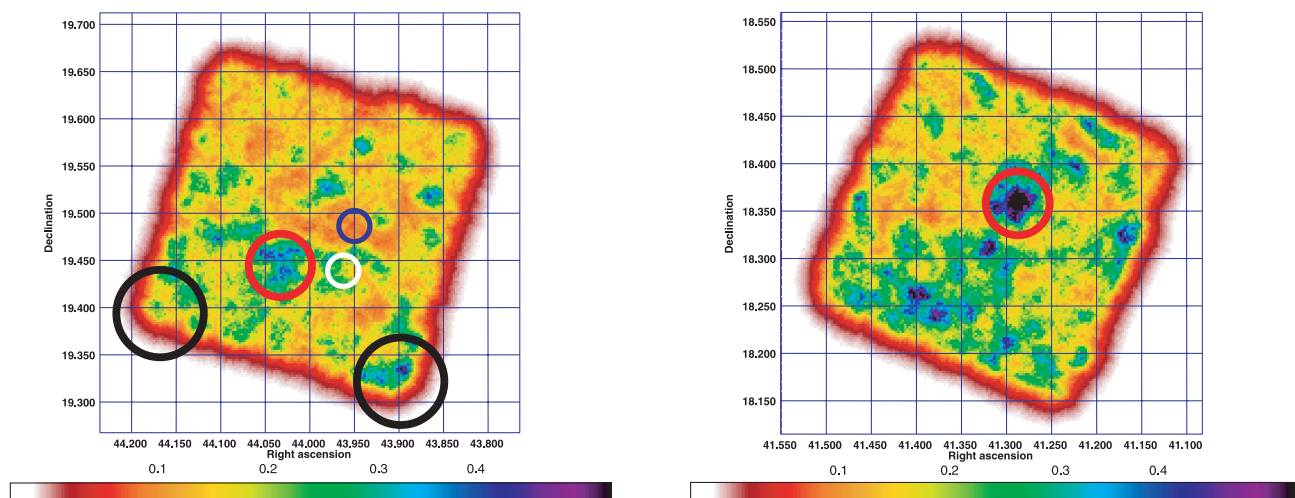

Fig. 2. (Left) MBM 12 field of view between 0.4–1.0 keV, after smoothing. Emission from XY Ari (red circle) can be seen, although the two weaker sources (blue, white circles) are not visible in this band. The black circles indicate the positions of the calibration sources. (Right) The off-cloud field of view, with an unidentified source (excluded in the analysis) marked with a $2'$ radius red circle.
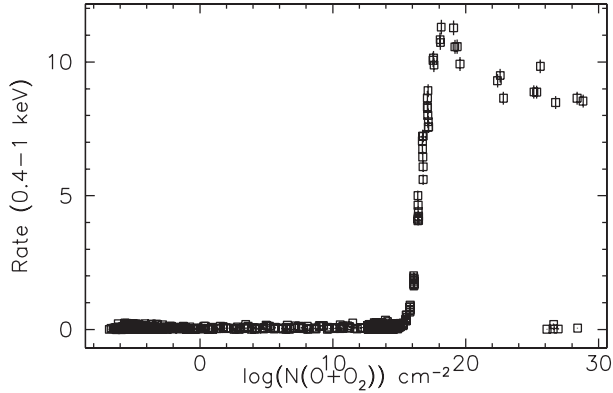
Fig. 3. The raw count rate in the 0.4–1.0 keV band for the on-cloud observation as a function of atmospheric column density of oxygen atoms and molecules. The scattered solar X-ray contribution rises sharply at low elevations, where the atmospheric column density of oxygen is larger than $\sim 10^{15}\,\mathrm{cm}^{-2}$.

Fig. 4. The count rate after standard filtering in the 0.4–1.0 keV band as a function of atmospheric column density of oxygen atoms and molecules.

2.1.2. Scattered solar X-rays

As Suzaku orbits the Earth maintaining a fixed pointing, the column density of atmosphere along the look direction varies rapidly. Solar X-rays can scatter off the atmosphere into the telescope, either via Thompson scattering or by fluorescence (Snowden, Freyberg 1993). Fluorescence of oxygen atoms and molecules is our greatest concern, as it would give rise to emission lines around 0.54 keV which could blend with the O VII line. We modeled the Earth's atmosphere using the NRLMSISE-00 empirical model (Hedin 1990), and combined this with the Suzaku orbital parameters to calculate the total solar-illuminated column density of oxygen atoms and O_2 molecules as a function of time.

We then extracted the count rate as a function of time in the 0.4–1.0 keV band and compared this to the oxygen column density N_O. In figure 3 we show the correlation plot for the uncleaned data. When the illuminated atmospheric N_O exceeds $\sim 10^{15}\,\mathrm{cm}^{-2}$, the count rate rises sharply due to scattered solar X-rays. We fit the data with N_O between 0–$10^{17}\,\mathrm{cm}^{-2}$ to a linear model and found that they are well described by the function $0.04 + (1.18 \pm 0.01) \times 10^{-16}\,N_O$ counts s^{-1}. In figure 4 we show the same plot (with a linear abscissa) after the standard filters are applied. All the lines of sight with column densities above $\sim 10^{14}\,\mathrm{cm}^{-2}$ have been eliminated (at least for this observation) by the requirements that the look direction be elevated by at least $10°$ and at least $20°$ away from the bright Earth terminator. Figure 4 shows that most times have either negligible oxygen column or $N_O \sim 10^{13}\,\mathrm{cm}^{-2}$. Applying our linear fit, we see that the integrated contamination due to fluorescent oxygen is less than ~ 0.001 counts s^{-1}. A similar result holds for the off-cloud observation as well. We therefore expect that the scattered solar X-ray contribution to our data is negligible.

2.1.3. Solar wind charge exchange

Diffuse soft X-ray emission can also be generated by ions in the solar wind interacting with neutral interplanetary or geocoronal material. However, the appearance and strength of emission lines emitted by SWCX is poorly characterized. It is expected that t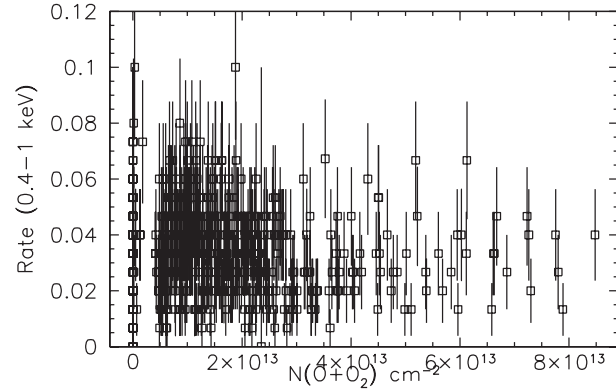he density, velocity, and ionization balance of the solar wind should correlate with the variable SWCX contribution, which is largely from the geocorona, but there may also be a more nearly constant component of the SWCX emission from interplanetary space. Figure 5 shows some of the relevant values for the two Suzaku observations and, for comparison, during an instance of strong SWCX emission seen by XMM-Newton.

Snowden, Collier, and Kuntz (2004) analyzed an XMM-Newton observation of the Hubble Deep Field North that showed substantial SWCX emission. That observation occurred during a period characterized by a strong solar proton flux (in only a few percent of observations are stronger fluxes seen), as well as high O^{+7}/O^{+6}, but low O^{+8}/O^{+7}. The proton speed was low, $\sim 350\,\mathrm{km\,s}^{-1}$. Enhanced O VII ($7.39 \pm 0.79\,\mathrm{LU}$) and (despite the low O^{+8}/O^{+7} ratio) O VIII ($6.54 \pm 0.34\,\mathrm{LU}$) emission was seen during this observation, along with a number of other species. In contrast, our Suzaku observations were done at a time characterized by a moderate proton flux in the solar wind, with the exception of one short period of the on-cloud observation. The O^{+7}/O^{+6} ratio during both observations was close to the mean ratio for the solar wind. The proton speed during both Suzaku observations was exceptionally low, typically $< 350\,\mathrm{km\,s}^{-1}$, which is seen in only a few percent of observations.

Nonetheless, there were some similarities in the solar wind parameters during the XMM-Newton observation that showed strong SWCX contamination and our Suzaku observations. In both, the solar wind was slow and dense. However, the peak proton flux during the Suzaku observations was less than half the proton flux responsible for the SWCX emission in the XMM-Newton observation, and the mean proton flux is even lower. Further, the XMM-Newton line of sight observed through the densest portion of the Earth's magnetosheath, whereas the Suzaku observations are through the flanks of the magnetosheath, thus further reducing the target neutrals with which the solar wind produces the X-ray emission. Unfortunately, our understanding of how the solar wind characteristics, satellite orbits, and observing directions interact to generate observed SWCX emission is still quite limited. Nonetheless, the combination of the solar wind strength and the look direction, as well as the fact that the ion ratios are close
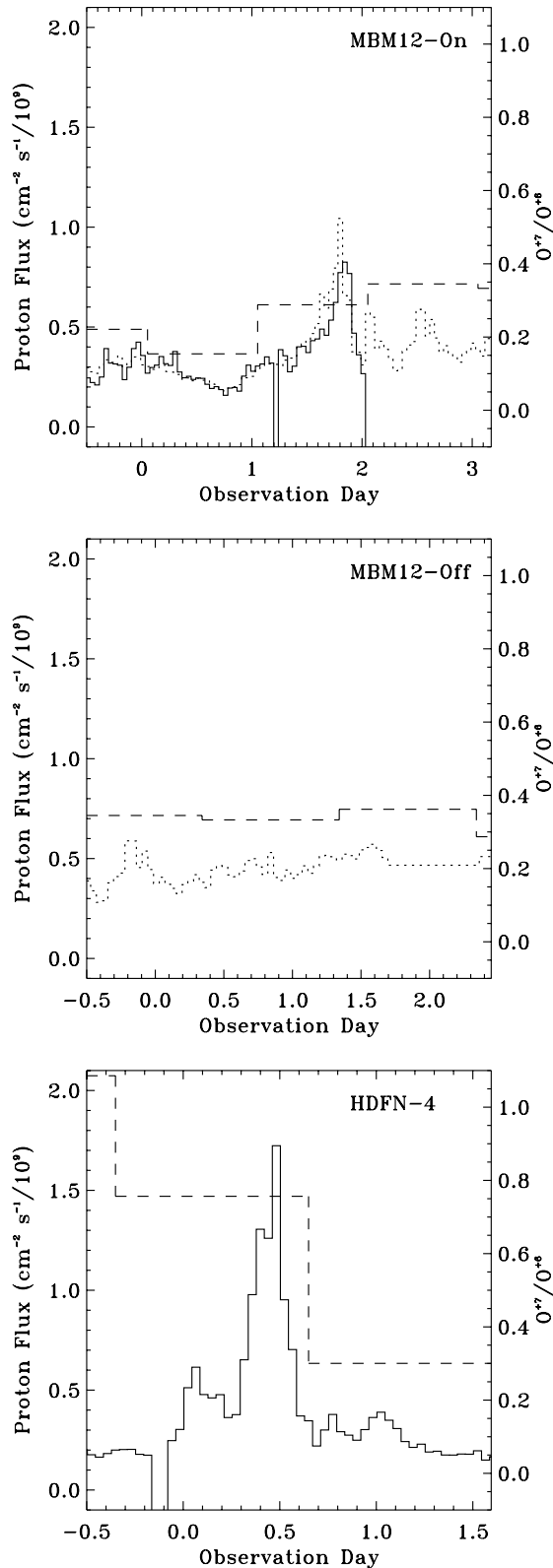
Fig. 6. The on-cloud spectrum between 0.4–1.0 keV (channels 110–273 in channel units). The best fit line plus Gaussian is shown.

to the mean values, suggests that whatever the SWCX surface brightness was during our Suzaku observations, it is typical for observations of the diffuse soft X-ray background.

2.2. XIS Response

For this work, we focused on the back-illuminated XIS 1 detector, which has the largest effective area of low energy X-rays. As these observations were performed early in the mission, very little degradation of the CCD response had occurred. Unfortunately, however, the time- and space-varying contamination layer which was discovered early in the mission has complicated observations at low energies (Koyama et al. 2007).

We calculated the XIS detector effective area using the tool xissimarfgen, which includes both the time and spatial effects of the contamination layer. We assumed a field-filling source, and used a detector mask which removed the bad pixel regions, along with the region excluded due to the bright source XY Ari. The model of the contamination layer is based on in-flight observations and has its own uncertainties. Combining these with other known sources of systematic error, we estimate that at 0.6 keV there is a $\sim 13\%$ systematic error on the final effective area $\times$ solid angle product, in addition to the given statistical errors.

3. Results

3.1. On-Cloud Emission

Although MBM 12 absorbs almost all distant emission below 0.7 keV, we cannot say if the foreground low energy emission is local to the solar system or tens of parsecs away. Our first goal, however, is to simply model the spectrum seen towards MBM 12 since this is likely the "darkest" high latitude line of sight in the Galaxy at soft X-ray energies.

3.1.1. Raw count model

The data clearly showed a feature near 0.56 keV, so we began by simply fitting a linear continuum plus a Gaussian to the observed count rates (with no background subtraction) for the on-cloud data on XIS 1 between 0.4–1.0 keV in PI channels. This approach is admittedly simplistic, but

Fig. 5. (Top) The hourly average value of the solar wind proton flux in units of $10^9\,\mathrm{cm}^{-2}\,\mathrm{s}^{-1}$ from the ACE (solid line) and WIND (dotted line) satellites (the ACE and WIND data have not been corrected for the time of flight to Suzaku). The daily average of the O^{+7}/O^{+6} ratio from ACE is shown by the dashed line. (Middle) Same, for the off-cloud observation. (Bottom) Same, shown for the Hubble Deep Field North XMM-Newton observation.
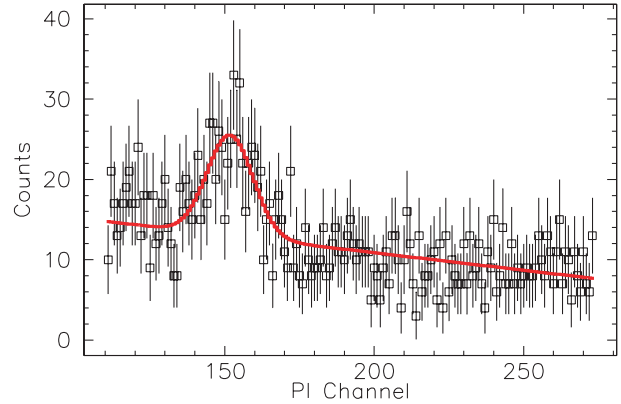
Table 1. Instrumental emission lines.

| Ion | E_{lab} | Night Earth | | | On-cloud | | |
| | | E | FWHM | S.B. | E | FWHM | S.B. |
	keV	keV	keV	LU	keV	keV	LU
Al K	1.49	1.48	0.044	0.28	1.48	0.044	0.28
Si K	1.74	1.74	0.053	0.36	1.74	0.053	0.36
Au M	2.123	2.13	0.170	0.34	2.13	0.170	0.34
Mn Kα	5.90	5.88	0.079	15.16	5.88	0.079	15.11
Mn Kβ	6.49	6.47	0.096	5.35	6.47	0.096	5.38

it gives a baseline measurement, useful when comparing to a more complicated physical model. Figure 6 shows the best-fit result, which has 229^{+34}_{-32} counts in the line and a centroid at PI channel 151.6 ± 1.0 or 553.3 ± 3.9 eV (using 3.65 eV/channel). Taking into account the area removed for bad pixels and the effects of the optical blocking filter contamination with a thickness appropriate for Day 209, Suzaku's effective area $\times$ solid angle product at 0.553 keV is 16875 cm^2 arcmin^2. With a total "good time" of 71.7 ks, we get a total surface brightness (S.B.) of 2.23 ± 0.32 LU. We also put a 2σ upper limit on any O VIII line (at 0.653 keV) of 20 counts (0.11 LU) using this method. Since the total number of counts is rather small, in this and all subsequent fits, we used the maximum likelihood Cash statistic (Cash 1979).

3.1.2. Physical model

To expand upon these simple results, we then considered a more realistic physical model which explicitly included the detector background along with known astrophysical sources. We restricted the energy range to 0.4–7 keV, as above 7 keV the particle background rises sharply. The background was fit to the night Earth data (see subsubsection 2.1.1) using a model consisting of the sum of a power-law, a constant, and the five emission lines expected in this energy range (see table 6.2 in the Suzaku Technical Description[2]). The emission lines were modeled as Gaussian profiles (see table 1). Note that the best-fit energies agree with the laboratory energies to within 1%. The variation in the FWHM is not completely understood, but the large value at 2.13 keV is probably due to the multiple lines found in the Au M complex. The power-law term (with best-fit $\Gamma = 1.02$ and amplitude 0.011 counts s^{-1} keV^{-1} at 1 keV) and the constant (amplitude 0.00723 counts s^{-1} keV^{-1}) were not folded through the effective area curve. These two terms account for the observed particle background, after the COR > 8 GV and ELV > 10° filters.

The source model included two absorbed broken power-laws to account for the cosmic X-ray background (CXRB) and an absorbed bremsstrahlung plus Fe line for the remaining XY Ari emission (see below). A Gaussian line was added to represent the blended N VI triplet and C VI Lyβ line, and a final Gaussian was included to represent the O VII emission. The broken power-law components fit the composite total AGN spectrum, giving a slope of 1.4 above 1.2 keV and steepening significantly below 1 keV as observed by ROSAT and Chandra (Hasinger et al. 1993; Mushotzky et al. 2000). The first broken power-law

was fixed with $\Gamma_1 = 1.54$, $\Gamma_2 = 1.4$, $E_b = 1.2$, and a normalization of 5.70 photons cm^{-2} sr^{-1} s^{-1} at 1 keV. The second broken power-law used fixed values of $\Gamma_1 = 1.96$, $\Gamma_2 = 1.4$, $E_b = 1.2$, but the normalization was allowed to vary below its nominal value of 4.90 photons cm^{-2} sr^{-1} s^{-1} at 1 keV; our best-fit value was 2.53 ± 0.36 photons cm^{-2} sr^{-1} s^{-1} at 1 keV. Both components were assumed to be absorbed with column density $N_{\mathrm{H}} = 4 \times 10^{21}$ cm^{-2}, using the value for MBM 12 found in Smith et al. (2005).

Despite the exclusion of the region within $2'$ of XY Ari from the spectrum, the source is so bright that its scattered emission contributes significantly to the overall spectrum above 1 keV. This contribution was modeled as absorbed bremsstrahlung emission with an additional iron line. The best-fit value had $N_{\mathrm{H}} = 5.5 \times 10^{22}$ cm^{-2}, $kT = 200$ keV, and a total absorbed surface brightness (0.4–7 keV) of 1.25×10^{-7} erg cm^{-2} s^{-1} sr^{-1}. The best-fit Fe line was at 6.98 keV, with FWHM 0.4 keV and surface brightness 1.3 LU. We note that, while this model fits the X-ray spectrum of XY Ari reasonably well, we do not claim it is a correct physical model of the emission. An initial fit to the XY Ari data itself (using data from the central $2'$) showed that the scattered flux is $\sim 22\%$ of the total source flux, in agreement with the expected value (19%) based on the XRT PSF after excluding the central $2'$. The best-fit temperature was lower ($kT = 45^{+19}_{-11}$ keV), and the absorption was higher ($N_{\mathrm{H}} = 6.7 \times 10^{22}$ cm^{-2}). The column density found for XY Ari is more than an order of magnitude larger than the MBM 12 value, although it is similar to the value found by Littlefair, Dhillon, and Marsh (2001), who used K-band spectroscopy to determine that XY Ari's secondary is an M0 V star, with an $A_V = 11.5 \pm 0.3$, corresponding to a hydrogen column density of 2.2×10^{22} cm^{-2}. However, Luhman (2001) showed that most stars within the MBM 12 cloud have $A_V < 2$, while background stars generally have values between $A_V = 3$–8. The origin of the discrepancy between these values and Littlefair, Dhillon, and Marsh (2001) is unknown, but may be due to an inadequate model for the X-ray spectrum of XY Ari. The absorbing material may be near XY Ari itself, although it is also possible that MBM 12 has a larger column density along this line of sight that the average value we assumed. This will not affect our results since our model already has little to no flux in the 0.5–0.7 keV band from beyond MBM 12. In any event, a more detailed analysis of the XY Ari data is in progress, and we are certain the effect on the continuum below 1 keV is small.

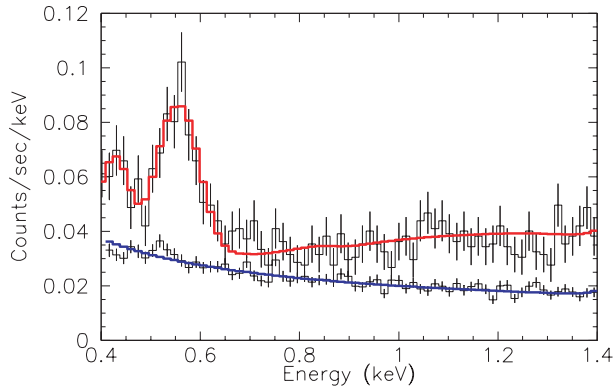[2] ⟨http://heasarc.gsfc.nasa.gov/docs/suzaku/prop_tools/suzaku_td/⟩.

Fig. 7. The on-cloud spectrum with the best-fit model with the background spectrum and best-fit model between 0.4–1.4 keV.
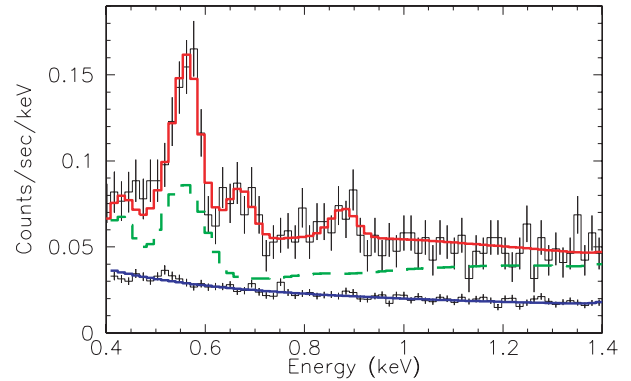

Fig. 8. The off-cloud spectrum and best-fit model (top), showing the three features at O VII, O VIII, and an unknown feature at 0.876 keV. The middle dashed curve shows the best-fit model for the on-cloud spectrum (data points omitted for clarity). The best-fit model for the night Earth data is at bottom.

The contribution from the Local Hot Bubble (LHB) itself is normally modeled as a thermal plasma in CIE with $T \sim 10^6$ K. However, most of the LHB emission is in the 0.1–0.3 keV bandpass, where Suzaku has some effective area but is not yet accurately calibrated. With our lower energy limit of 0.4 keV, the only strong lines expected from the LHB are from the N VI triplet at ~ 0.43 keV, along with C VI Lyβ emission at the same energy. We therefore included a single Gaussian to represent these lines, and ignored the continuum since this is negligible in a thermal plasma with $T \sim 10^6$ K. The best-fit position was 0.42 ± 0.03 keV, with FWHM 0.058 keV and surface brightness $2.4^{+2.2}_{-0.60}$ LU.

The final term was a Gaussian to represent the oxygen emission. The best-fit parameters put the line at 0.556 ± 0.003 keV, with FWHM 0.071 keV and a total surface brightness of 3.53 ± 0.26 LU. The line position is nearly identical to that found in subsubsection 3.1.1, while the surface brightness is increased by 60%. In this model, the continuum (due to particle background, the tail of the CCD response, and the absorbed CXRB) is very low at the O VII line, as opposed to the simple model which assumed a flat continuum under the line. The best-fit spectrum, including the background night Earth data, is shown in figure 7.

In the simple model, we were able to put a 2σ upper limit on any O VIII contribution by adding a delta function at the expected position of an O VIII line. Likewise here we added a delta function to the model at 0.653 keV, to represent the O VIII Lyα line. The best-fit result is a marginal detection of a feature with surface brightness 0.24 ± 0.1 LU, which when included in the model reduces the O VII surface brightness to 3.34 ± 0.26 LU. The O VIII/O VII surface brightness ratio is then $7.2 \pm 3.0\%$. Smith et al. (2005) noted that the O VII $n = 3 \rightarrow 1$ transition (at 0.666 keV) line can contribute as much as 6% of the flux of the main O VII $n = 2 \rightarrow 1$ triplet. Although we do not claim this as a detection, it seems more likely that this emission is from this O VII line and not O VIII.

3.2. Off-Cloud Emission

The off-cloud observations were taken immediately following the on-cloud data and as shown in subsubsection 2.1.3, the solar wind parameters were relatively stable during this period. So assuming the SWCX contribution is stable, we can use the difference between these observations as an estimate of distant Galactic disk and halo emission.

We assumed the "background" (actually a foreground in this case) for the off-cloud spectrum is the same as the on-cloud spectrum without the contribution from XY Ari. We assume that the "distant" emission originates beyond most of the Galactic gas (with $N_H = 8.7 \times 10^{20}$ cm^{-2}) seen in this direction. Figure 8 shows the best-fit to the off-cloud spectrum between 0.4–1.5 keV. We added two Gaussian lines to the model to represent the "distant" emission from O VII and O VIII, as well as a third (with FWHM set to 0 to force the fit to reflect a single line, rather than a very wide blend) to fit the excess between 0.85–0.9 keV. The "local" oxygen emission lines measured in the on-cloud observation were also included in this fit, so these new lines measure only the "distant" component. The fit parameters are given in table 2. The O VII $n = 3 \rightarrow 1$ line (at 0.666 keV) may contribute up to 6% of the O VII emission ($\lesssim 0.14$ LU) to the O VIII feature. This line could also be responsible in part for shifting the best-fit line energy above 0.653 keV, the energy of the O VIII Lyα line. Nonetheless, the majority of the emission at 0.668(6) keV must be from O VIII, as it is the only strong line near this energy.

The O VIII detection indicates that the distant plasma is either hotter or more out of equilibrium than the LHB plasma. In either case, the 0.7–1.3 keV range may contain relatively weak emission from Neon and Fe L shell lines. To put a limit on any such emission, we added a delta function to the model at 0.826 keV (15.01 Å), where the strongest Fe feature, from Fe XVII, would be expected. The 2σ upper limit on the Fe XVII line is 0.19 LU. This is not unexpected, since the expected surface brightness in this line is only $\sim 3\%$ of the O VIII value assuming an Fe/H abundance of 3.24×10^{-5} and a temperature of $\sim 2 \times 10^6$ K (see subsection 4.2). This reinforces the confusing nature of the unknown feature at 0.876 keV, since its origin is therefore almost certainly not Fe L shell emission.

R. K. Smith et al.

Table 2. Best-fit parameters for distant emission, with 1σ errors.[*]

Ion	Energy keV	FWHM keV	Flux LU
O VII	0.562(4)	< 0.001	2.34 ± 0.33
O VIII	0.668(6)	0.02(2)	0.77 ± 0.16
Unknown	0.876(9)	0	0.26 ± 0.08

[*] Value in parentheses shows error on the last digit.

4. Discussion and Conclusions

4.1. On-Cloud

By observing both MBM 12 and a nearby "off-cloud" field in quick succession with a low-background imaging X-ray spectrometers, we can reliably measure both the foreground and distant emission. Our on-cloud result indicates a rather high value for the "local" diffuse O VII surface brightness of about 3.5 LU. This emission is almost certainly generated in front of MBM 12 since the cloud is optically thick, with transmission < 3% at O VII. Assuming the O VII surface brightness behind MBM 12 is the same as the value given in table 2, the background contribution to the on-cloud emission is < 0.06 LU. As first suggested by Cox (1998), the most likely sources for the foreground emission are either the LHB, SWCX, or both.

Although larger than expected for standard LHB models, the local O VII surface brightness is still lower than most measured values towards high-latitude sightlines. McCammon et al. (2002) found 4.8 ± 0.8 LU of O VII towards a 1 sr region at high latitude, while the 2σ upper limit set toward MBM 12 by Snowden, McCammon, and Verter (1993), with ROSAT is equivalent to 7.1 LU at O VII. ASCA observations towards high-latitude sightlines found a surface brightness of 2.3 ± 0.3 LU in O VII, although this was model dependent (Gendreau et al. 1995).

Smith et al. (2005) did find a lower value for the local O VII surface brightness ($1.92^{+0.61}_{-0.60}$ LU, statistical errors only) when observing MBM 12 with Chandra. However, Chandra's particle background is both larger and more uncertain than Suzaku's. In addition, a large solar flare occurred during the Chandra observation, and Smith et al. (2005) noted that this increased the uncertainty. Smith et al. (2005) also measured an O VIII surface brightness of $2.35^{+0.59}_{-0.43}$ LU, which they attributed largely to SWCX particle background (along with an unknown portion of the O VII emission). We find a marginal detection of 0.24 ± 0.1 LU of O VIII towards MBM 12. It seems likely that including the poorly-understood systematic errors on the Chandra O VII result would bring it into agreement with the Suzaku measurement, although we cannot say with precision how much of either is due to SWCX and not the LHB. In contrast, the O VIII seen with Chandra is almost certainly due to SWCX (Smith et al. 2005).

It is difficult to generate the observed O VII surface brightness from a solar abundance LHB model consistent with ROSAT and other observations, as a model that generates the observed O VII emission will predict too much 1/4 keV band emission. As described in Smith et al. (2005), the dominant source of O VII flux in a thermal plasma is collisional excitation of O^{+6} ions, unless the plasma is substantially out of equilibrium. We are, however, reasonably certain the LHB is near equilibrium. The strongly recombining model proposed by Breitschwerdt and Schmutzler (1994) was ruled out by Smith et al. (2005). They showed that the 2σ upper limits to the O VII and O VIII surface brightnesses from the Chandra MBM 12 observation, combined with upper limits on the O VI surface brightness from FUSE (Shelton 2003) and the ROSAT All-Sky surface 1/4 keV band brightness (Snowden et al. 1995) excluded this type of model. Conversely, Edgar and Cox (1993) considered models of the LHB arising from a strongly ionizing plasma, created by a recent supernova. They concluded that generating the observed soft X-ray emission required an unrealistically high ambient ISM pressure ($p/k > 3 \times 10^4$ cm^{-3} K). In addition, these types of models typically predict significant amounts of high-velocity O VI, which have not been observed (Shelton 2002).

We therefore consider models in collisional equilibrium. A CIE plasma at 10^6 K, the "typical" temperature for the LHB (SMV 93), has an O VII triplet emissivity of $\Lambda = 5.7 \times 10^{-16}$ photons cm^3 s^{-1}, assuming the oxygen abundance relative to hydrogen is 8.51×10^{-4} (Smith et al. 2001). This rises rapidly with temperature, reaching 1.5×10^{-15} photons cm^3 s^{-1} at 1.2×10^6 K, and peaking (for $T = 2 \times 10^6$ K) at 6.4×10^{-15} photons cm^3 s^{-1}. However, the 2σ upper limit on the O VIII/O VII ratio of 13% puts an upper limit on the equilibrium temperature of 1.7×10^6 K (where $\Lambda = 4.8 \times 10^{-15}$ photons cm^3 s^{-1}).

Using these values, and assuming a constant density and temperature throughout the LHB, we can express the total surface brightness of O VII as:

$$L_S(\text{O VII}) = \frac{1}{4\pi} R_{\text{LHB}} \frac{n_e^2}{1.2} \Lambda_{\text{O VII}} \tag{1}$$

where L_S is in LU, n_e is the electron density, and R_{LHB} is the bubble radius. This assumes that hydrogen and helium are fully ionized, so $n_e \approx 1.2 n_H$. Taking our lower value of 2.3 LU of O VII, equation (1) gives $n_e^2 R_{\text{LHB}} = 0.020$ cm^{-6} pc at 10^6 K, or 0.0075 cm^{-6} pc at 1.2×10^6 K. We can obtain a lower limit of 0.0023 cm^{-6} pc on this value using our upper limit of $T = 1.7 \times 10^6$ K. This final value is similar to the emission measure found by SMV 93 (0.0024 cm^{-6} pc), although at a significantly higher temperature. Assuming $R_{\text{LHB}} = 100$ pc, we require electron densities of 0.014, 0.0087, or 0.0048 cm^{-3}, and a pressure of $p/k = 3.0$, 2.2, or 1.7×10^4 cm^{-3} K at $T = 10^6$ K, 1.2×10^6 K, or 1.7×10^6 K, respectively.

Interestingly, Cox (2005) found that the midplane pressure required to support the various layers of the Galaxy (e.g. cold and warm H I, diffuse H II, etc) is 2.2×10^4 cm^{-3} K, in agreement with our value at $T = 1.2 \times 10^6$ K. In addition, Snowden et al. (2000) used X-ray shadows (such as those created by MBM 12) seen in the ROSAT All-Sky Survey observations at 1/4 keV to measure the temperature of the local diffuse soft X-ray component. They also found a best-fit temperature of 1.2×10^6 K, although this is based on the Raymond and Smith (1977, RS77) plasma code. In particular, using this temperature and the pressure with the 1993 update to the RS77 plasma code (using solar abundances) would predict

$\sim 3\times$ the observed 1/4 keV band surface brightness seen by ROSAT. This could perhaps be explained if the Si, Fe, and other high-Z elements that create the 1/4 keV band emission were depleted relative to oxygen in the LHB; more modelling is needed to test this hypothesis.

Despite the suggestive agreement in temperature and pressure described above, there are issues in other wavebands. Hurwitz, Sasseen, and Sirk (2005) has placed a 95% upper limit on the emission measure of a local 10^6 K component of 0.0004 cm^{-6} pc, based on CHIPS observations of diffuse EUV iron lines and assuming a solar abundance for iron. Even if iron is fully depleted, they still find a 95% upper limit of ~ 0.005 cm^{-6} pc for any CIE model with $T < 1.6 \times 10^6$ K, based on the non-detection of O V and O VI lines near 171–173 Å.

The fully-depleted Hurwitz, Sasseen, and Sirk (2005) upper limit disagrees with our value of 0.0075 cm^{-6} pc by a factor of at least 50%. In addition, the solar-abundance CHIPS limit strongly disagrees with the value found by SMV 93 and from the ROSAT All-Sky Survey in the 1/4 keV band (~ 0.0018–0.0058 cm^{-6} pc) which also assumes solar abundances (Snowden et al. 1998). Hurwitz, Sasseen, and Sirk (2005) noted these discrepancies and suggested that some depleted abundance pattern might exist that brings the X-ray and EUV observations into agreement. Nonetheless, as it stands the fully-depleted CHIPS limits suggest that at least a third of the O VII we detect is not from the LHB. One possibility is that this emission comes from SWCX. More analysis of the solar wind data will be needed to determine if the observations were truly done during a period of relative quiescence; for example, the absolute O^{+7} and O^{+8} fluxes can be derived from ACE data with additional effort. While figure 5, based on the automatically processed ACE data, does not show any signs of increased oxygen flux, more data are needed to confirm this.

4.2. "Distant" Emission

Figure 5 shows that the solar wind conditions were similar during both observations, and the LHB intensity is not expected to change over an angle of less than 3°. If both oxygen lines are from an unabsorbed plasma in CIE, the O VIII/O VII ratio (0.33 ± 0.08) implies $T = (2.2^{+0.1}_{-0.2}) \times 10^6$ K. At this temperature, the predicted emission measure is $(1.9 \pm 0.3) \times 10^{-3}$ cm^{-6} pc

using ATOMDB ver. 1.3.1 emissivities (Smith et al. 2001). If, as is more likely, the plasma is behind the Galactic hydrogen layer ($N_H = 8.7 \times 10^{20}$ cm^{-2}), then the unabsorbed O VIII/O VII ratio would be 0.26 ± 0.06. In this case, $T = 2.1 \pm 0.1 \times 10^6$ K and the emission measure is $(4.0 \pm 0.6) \times 10^{-3}$ cm^{-6} pc. In either case, our results are consistent with previous measurements of distant hot halo gas. However, our result does not touch on the question of whether the halo has one (Pietz et al. 1998) or two (Kuntz, Snowden 2000) dominant temperatures; further Suzaku observations will be necessary to address this question.

The line at 0.876 keV is a mystery, although we stress it is at best a 3σ detection. Between 0.7–1.3 keV, the strongest emission lines in a collisional plasma are typically from neon or iron. The closest strong neon line to 0.876 keV is the Ne IX forbidden line, but this would require a 5% gain error in the XIS 1. The oxygen lines at lower energies show $< 2\%$ gain shift, and the calibration lines at higher energies (see table 1) have less than 1% gain shift. The strongest iron lines near this energy are from $2p^4 3d \to 2p^5$ transitions in Fe XVIII, but any identification with an Fe line is problematic since many other lines of Fe XVIII (such as the $2p^4 3s \to 2p^5$ line at 0.775 keV) would also be expected. In particular, the 2σ upper limit on the Fe XVII 0.826 keV line of 0.19 LU strongly limits any Fe line identification for the line at 0.876 keV. It is possible it is an as-yet unidentified weak instrumental line, although this raises the question of why it is not present in the on-cloud data.

Intriguingly, the Lyman limit for O VIII is 0.8704 keV, so it is possible that this is not a line, but rather a recombination edge resulting from cool electrons interacting with O^{+8} ions. If so, we wonder at the origin of the O^{+8} ions — are they local to the solar system due to a sudden change in the solar wind during the off-cloud observation, or from a distant recombining plasma? As more data from ACE and Suzaku become available, we may be able to answer this question.

References

Bhardwaj, A. 2006, Adv. Geosci. in press (astro-ph/0605282)

Breitschwerdt, D., & Schmutzler, T. 1994, Nature, 371, 774

Cash, W. 1979, ApJ, 228, 939

Cox, D. P. 1998, in Lecture Notes in Physics 506, The Local Buble and Beyond, ed. D. Breitschwerdt, M. J. Freyberg, & J. Trümper (Berlin: Springer Verlag), 121

Cox, D. P. 2005, ARA&A, 43, 337

Edgar, R. J., & Cox, D. P. 1993, ApJ, 413, 190

Gendreau, K. C., et al. 1995, PASJ, 47, L5

Hasinger, G., Burg, R., Giacconi, R., Hartner, G., Schmidt, M., Trümper, J., & Zamorani, G. 1993, A&A, 275, 1

Hedin, A. E. 1990, J. Geophys. Res., 96, 1159, 1991

Hurwitz, M., Sasseen, T. P., & Sirk, M. M. 2005, ApJ, 623, 911

Koyama, K., et al. 2007, PASJ, 59, S23

Kuntz, K. D., & Snowden, S. L. 2000, ApJ, 543, 195

Kuntz, K. D., & Snowden, S. L. 2001, ApJ, 554, 684

Lallement, R. 2004, A&A, 418, 143

Littlefair, S. P., Dhillon, V. S., & Marsh, T. R. 2001, MNRAS, 327, 669

Luhman, K. L. 2001, ApJ, 560, 287

McCammon, D., et al. 2002, ApJ, 576, 188

McCammon, D., Burrows, D. N., Sanders, W. T., & Kraushaar, W. L. 1983, ApJ, 269, 107

McCammon, D., & Sanders, W. T. 1990, ARA&A, 28, 657

Mushotzky, R. F., Cowie, L. L., Barger, A. J., & Arnaud, K. A. 2000, Nature, 404, 459

Pietz, J., Kerp, J., Kalberla, P. M. W., Burton, W. B., Hartmann, D., & Mebold, U. 1998, A&A, 332, 55

Raymond, J. C., & Smith, B. W. 1977, ApJS, 35, 419 (RS77)

Salinas, A., & Schlegel, E. M. 2004, AJ, 128, 1331

Shelton, R. L. 2002, ApJ, 569, 758

Shelton, R. L. 2003, ApJ, 589, 26

Smith, R. K., Brickhouse, N. S., Liedahl, D. A., & Raymond, J. C. 2001, ApJ, 556, L91

Smith, R. K., Edgar, R. J., Plucinsky, P. P., Wargelin, B. J., Freeman, P. E., & Biller, B. A. 2005, ApJ, 623, 225

Snowden, S. L., et al. 1995, ApJ, 454, 643

Snowden, S. L., Collier, M. R., & Kuntz, K. D. 2004, ApJ, 610, 1182

Snowden, S. L., Cox, D. P., McCammon, D., & Sanders, W. T. 1990, ApJ, 354, 211

Snowden, S. L., Egger, R., Finkbeiner, D. P., Freyberg, M. J., & Plucinsky, P. P. 1998, ApJ, 493, 715

Snowden, S. L., & Freyberg, M. J. 1993, ApJ, 404, 403

Snowden, S. L., Freyberg, M. J., Kuntz, K. D., & Sanders, W. T. 2000, ApJS, 128, 171

Snowden, S. L., McCammon, D., & Verter, F. 1993, ApJ, 354, 211 (SMV93)

Tanaka, Y., & Bleeker, J. A. M. 1977, Space Sci. Rev., 20, 815